

Moon echoes from the 53 MHz MST radar at Gadanki, India

A. K. Patra* and T. Rajendra Prasad

National Atmospheric Research Laboratory, Gadanki 517 112, India

In this article we describe the first results from the Moon echo experiment conducted using the 53 MHz MST radar located at Gadanki, India. Observations show that echoes are as strong as 20 dB above noise and these are related to radar returns at normal incidence from places close to the sub-terrestrial point on the Moon. Spectral features of these echoes are narrow, indicating the dominance of quasi-specular scattering process. At higher range, which is also related to higher incidence angle, echo power is found to remarkably decrease. These echoes are characterized with multiple spectral peaks and broader spectral features. Higher-order spectral analysis suggests that multiple spectral peaks are due to discrete multiple scattering centres. Initial results are found to be in agreement with those reported earlier at similar frequencies and are promising. Implications of these results along with the potential and future prospect of the Gadanki MST radar for Earth-based planetary research are discussed.

Keywords: Echo, Moon, MST radar, spectral features.

RADAR techniques have been extensively used for studying the Moon ever since the first echoes from the Moon were detected using ground-based radar¹. Both Earth- and satellite-based radar techniques have since been employed for probing the Moon's surface topography, impact craters morphology, and regolith²⁻⁷. Radar techniques have also been used for finding ice on the Moon^{8,9}, although from the view point of radar probing of the Moon this issue continues to remain unresolved¹⁰.

Most of the radar observations for studying the Moon, however, have been made at centimetre wavelength⁵, except for a few which were done from the Earth in the metre-decametre wavelength^{2,3,11,12}. Radar experiments at metre-decametre wavelengths provided important information on the wavelength dependence of radar cross-section and angular dependence of backscattering, which was used for characterizing lunar surface properties, regolith and underneath rocks¹⁰.

On the other hand, Moon echoes have traditionally been used to characterize large phased array VHF atmospheric radars^{13,14}, but no attempt has been made to char-

acterize these echoes. Given the fact that surface roughness of the Moon at scales comparable to radar wavelength is one of the important factors that influences radar echoes¹⁰, characterization of Moon echoes at VHF frequencies assumes significance.

We explored the possibility of detecting Moon echoes using the Mesosphere–Stratosphere–Troposphere (MST) radar, located at National Atmospheric Research Laboratory, Gadanki (13.5°N, 79.2°E; hereafter referred to as Gadanki MST radar), Andhra Pradesh, India. The Gadanki MST radar operates at 53 MHz with a maximum peak power of 2.5 MW and antenna aperture of $1.7 \times 10^4 \text{ m}^2$. It was primarily designed to detect echoes from refractive index variations present in the Earth's neutral atmosphere and ionosphere for studying various dynamical processes therein^{15,16}. For the Moon echo experiment, our objectives were twofold: (1) to detect and characterize Moon echoes, and (2) to use the Moon for characterizing the antenna pattern of the Gadanki MST radar. Here, we describe the experiment and first results of Moon echoes, including their spectral features.

Experiment description

Gadanki MST radar observations of Moon echoes reported here were performed on 31 December 2014, when the transit of the Moon was over the radar field of view. On this day, the Moon arrived over zenith at 20:28 IST (UT+5:30 h). Considering that radio experiment could suffer from scintillation effect by ionospheric plasma irregularities associated with equatorial plasma bubble that occur in the evening, we monitored the presence/absence of ionospheric irregularities using a collocated state-of-the-art digisonde, so that their effects on the observations can be accounted for. Ionospheric irregularities were absent during the experiment. Faraday rotation effect, if any, due to magnetized plasma in the intervening medium on the linear polarization used in the experiment (both in transmission and reception), however, could not be avoided.

Table 1 shows the radar parameters used in the experiment. Note that the inter-pulse period (IPP) of 2.7 ms (unambiguous radar range of 405 km), however, is not sufficient for measuring the range between the radar and the Moon surface, which is about 368,000 km. The RF

*For correspondence. (e-mail: akpatra@narl.gov.in)

pulse has to travel for ~ 2.5 sec to return to the radar from the surface of the Moon. Thus in the present case the range measurement is aliased due to range folding linked with the short IPP used in the experiment. The short IPP (2.7 ms) and coherent integration (four in the present case), however, have facilitated us to detect Moon echoes with a sampling rate of 92.6 Hz (i.e. $1/(2.7 \text{ ms} \times 4)$) for Doppler spectral measurement. This provided a Doppler window (i.e. Nyquist frequency) of ± 46.3 Hz.

We have also used a pulse length (τ) of $32 \mu\text{s}$, which is shorter than those used earlier for similar measurements made from other ground-based radar sites. This has provided us measurements of echo power and spectral properties at every 4.8 km ($c\tau/2$, where $c = 3 \times 10^8 \text{ m s}^{-1}$ is the velocity of light) interval from different parts of the Moon as the radar pulse travels. Figure 1 shows the relevant geometry illustrating how a pulsed radar experiment provides information regarding the Moon as it travels from the sub-terrestrial point P to the limbs of the Moon. In this way, the radio pulse of duration τ (which is $32 \mu\text{s}$ in

the present case) travelling with the velocity of light c illuminates an annular ring of area $A (= 2\pi Rc\tau)$ on the surface of the Moon, where R is the average radius of the Moon. The area of the annular ring depends on the pulse length τ and hence shorter the pulse length, better is the resolution. The angle of incidence θ (which is based on the assumption that the Moon is a smooth sphere), however, changes from 0° to 90° as the pulse travels. While this aspect should be kept in mind when interpreting echoes coming from different ranges, it is also important to note that the Moon is not a smooth spherical body but comprises of complex terrain and regolith. Thus back-scattered echoes are expected even when the angle of incidence is non-zero.

The radar beam was positioned at east- 18° , east- 12° , east- 6° , zenith, and west- 6° sequentially so as to receive Moon echoes, while it was apparently transiting from east to west. Given that the antenna beam width (3 dB full width) of the Gadanki MST radar is 2.8° and the apparent angular dimension of the Moon is about 0.5° , the transit time of the Moon across the antenna beam is estimated to be about 15 min. For the observations presented here, however, data were collected for 26 min at each beam position to detect echoes, if any, at angles beyond the 3 dB width of the antenna radiation pattern.

Echoes from four consecutive pulses were coherently integrated and time-series data, each consisting of 2048 points forming a data length of 22.12 s (i.e. $2.7 \text{ ms} \times 4 \times 2048 = 22.12 \text{ s}$), in the form of in-phase and quadrature components were stored for post-processing. Spectral estimation was performed offline using fast Fourier transform (FFT) on 2048 data points providing spectral observations in a Doppler window of ± 46.3 Hz and spectral resolution of 0.045 Hz (i.e. $92.6 \text{ Hz}/2048$).

Table 1. Radar specifications and other important parameters used in the present experiment

| Parameter | Value |
|----------------------------------|---|
| Frequency | 53 MHz |
| Peak power | 1.8 MW |
| Antenna aperture | $1.7 \times 10^4 \text{ m}^2$ |
| Half power full beam width | 2.8° |
| Pulse width | $32 \mu\text{s}$ |
| Inter-pulse period | 2.7 ms |
| No. of coherent integrations | 4 |
| No. of time-series data points | 2048 |
| No. of range bins | 80 |
| Beam direction | East- 18° , east- 12° , east- 6° , zenith, west- 6° |
| Dwell time in each beam position | 26 min |
| Data recording mode | Complex time series (in-phase and quadrature components) |

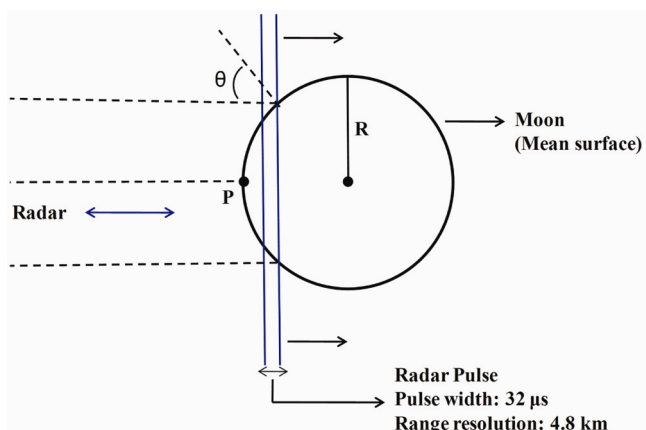


Figure 1. Geometry of radar backscatter from the Moon. As the radar pulse travels, the angle of incidence changes and it covers different annular areas on the Moon surface.

Observational results

Range distribution of Moon echo power

Figure 2 shows range-time variations of signal-to-noise ratio (SNR) of Moon echoes observed in different beam positions. Noise power is reckoned over the coherent integration filter bandwidth of 92.6 Hz. Echoes marked as A, B, C, D, and E correspond to observations made in the east- 18° , east- 12° , east- 6° , zenith, and west- 6° beams respectively. As mentioned earlier, echo range is aliased due to the selection of short IPP (2.7 ms). Nonetheless, the composite echo pattern constructed from all observations clearly depicts motion of the Moon towards and away from the radar location. Note that the closest range occurs when the beam zenith angle is east- 6° instead of zenith and the cosine-like pattern is suggestive of near east-west motion of the Moon in a limited observational field of view (i.e. between east- 18° and west- 6°) of the Gadanki MST radar used in the present experiment.

Echoes are as strong as 20 dB above noise. Strong echoes are found in the first few range gates when the radio pulse is close to the sub-terrestrial point on the Moon and as the radio pulse travels further, echo power decreases.

Figure 3 provides more details on the variations of echo power with range (i.e. time delay). Echo powers observed at different range gates are normalized to the received peak power in the entire range window, which came presumably from normal incidence. As the figure shows, echo power falls off fast after two range gates (which cover 64 μs in time and hence 9.6 km in range) and echo power is reduced by 80% in the next 8–10 range gates and by 90% in the subsequent range gates. This change in echo power with range can also be viewed as angular dependence of echo power, since the angle of incidence changes as the pulse travels. For short pulse (such as 32 μs used here), the role of quasi-specular component is expected to decrease as the pulse travels

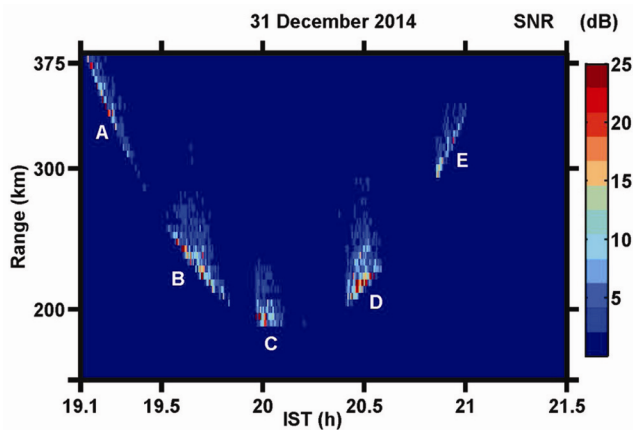


Figure 2. Signal-to-noise ratio (SNR) of Moon echoes as a function of range and time observed in different beams. Echoes marked as A, B, C, D, and E correspond to observations made in the east-18°, east-12°, east-6°, zenith, and west-6° beams respectively.

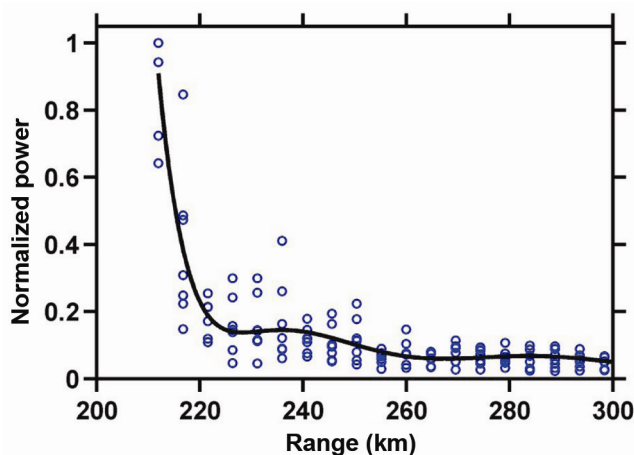


Figure 3. Echo power variations with range as the radar pulse travels from the sub-terrestrial point to the limb of the Moon. Echo power is normalized to the maximum power observed in a given frame.

towards the limbs from the sub-terrestrial point. Strong echoes observed in the first two range gates are due to dominance of quasi-specular component from smooth surfaces having large spatial correlation at normal incidence, while the weak echoes observed in the subsequent range gates are possibly due to multiple reflections from rough surface features (rocks and jagged facets) capable of reflecting radio waves at large incidence angle. At large incidence angle, the rough surface features are expected to dominate and tend to scatter in isotropic fashion, which can be noticed in the variation of echo power with range. Results presented here are in agreement with some of the early radar measurements made by Klemperer¹¹ at a wavelength of 6 m and by Davis and Rohlfis¹² at a wavelength of 11.3 m.

Doppler spectral behaviour

Figure 4 *a–c* shows Doppler power spectra observed in east-12°, east-6° and zenith beams respectively. Mean Doppler in a given beam position is found to be identical at every range gate, clearly exemplifying the mean motion of the Moon, irrespective of the echoing processes. The mean Doppler shifts in east-12°, east-6° and zenith beams are +15, +3.8 and –14.5 Hz respectively, representing apparent westward transit of the Moon.

Figure 5 provides a summary of all spectral data, in the form of line-of-sight (LOS) mean Doppler velocity and Doppler spectral width. These are estimated using moments method and represent $-\lambda/2$ times the mean Doppler (the first moment) and $\lambda/2$ times the square root of variance (second moment), where $\lambda = 5.66$ m is the radar wavelength. Mean Doppler velocity and Doppler spectral width are in the range -50 to 50 m s^{-1} and 10 to 40 m s^{-1} respectively. Positive (negative) velocity represents motion away from (towards) the radar. Note that mean

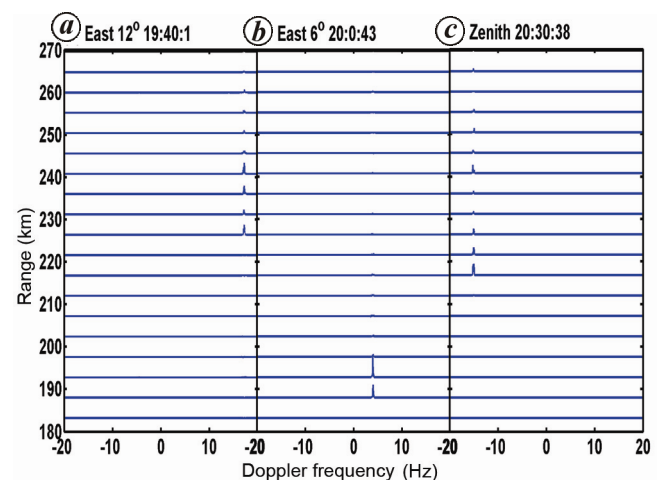


Figure 4. Doppler power spectrum observed in (a) east-12°, (b) east-6° and (c) zenith beams.

Doppler velocities observed in east-18° to east-6° beams show motion towards the radar, and those observed in zenith and west-6° beams show motion away from the radar. Near-zero velocity is observed when the beam is positioned at east-6°. One can also notice change in velocity in a given beam as time elapses.

Doppler spectral width is minimum for strong echoes, which come from the first few range gates, and the spectral width is higher for echoes coming from higher ranges. Further, spectral width is found to vary with beam position. When the radar beam is at east-6° and zenith, the spectral width is minimum. It may be recalled that LOS velocity close to zero is observed in the east-6° beam.

In order to understand the spectral features further, we take a closer look of the spectral data (Figure 6). Figure 6a and b shows zoomed version of Doppler spectra observed in the east-6° and zenith beams respectively. On the right side of each panel is the corresponding normalized echo power (normalized to peak power in the frame). It is clear that echoes in the first two range gates are strong and spectra are less structured than those observed in the subsequent ranges. Less power and more structured spectra could be due to echoes originating from multiple discrete targets. It may be noted from Figure 6b that echo power corresponding to the spectrum marked as S2 is about 60% that of S1 and is remarkably higher than those observed in the adjacent range gates.

In order to understand the behaviour of the spectral data marked as S1 and S2, we have closely examined temporal behaviour of time-series data and its frequency components. Figure 7a and b illustrates results corresponding to spectral data marked as S1 and S2 respectively in Figure 6b (zenith beam data). The panels from

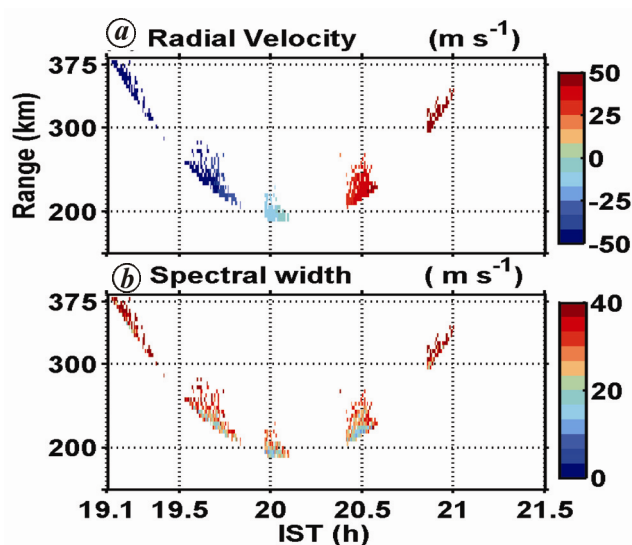


Figure 5. (a) Mean Doppler velocity and (b) Doppler spectral width observed with range and time in different beams.

top to bottom represent time-series data (in-phase channel), Doppler power spectrum (only the negative part of the spectrum is shown), zoomed version of power spectrum and bi-spectrum respectively. Note that in the first 2.5 sec of the time-series data, there is no echo as expected. The fading rates of the signal corresponding to S1 and S2 are different; faster fading is observed in the case of S2 compared to S1. Here it may also be mentioned that fading observed in the case of S2 is somewhat faster than those observed in the rest of signals. With regard to the Doppler spectrum, both show two dominant peaks, but in the case of S2, the peaks are well separated. There are also additional spectral peaks, but they are less significant. Similar multi-peak spectra were reported earlier by Davis *et al.*¹⁷ based on radar observations made at 11.3 m wavelength. Given the fact that signals linked with S2 come from the limbs of the Moon, signals could come from discrete targets satisfying quasi-specular reflection properties.

To find to what extent these peaks are independent and localized, we performed wavelet and bi-spectrum analysis of signals. Wavelet analysis has been performed to study stationarity of signal, which reveals the temporal variations of frequencies present in the signal. Wavelet spectrum (not presented) clearly show stationarity of signal throughout the observations, but the time resolution of the dataset does not permit to resolve the closely separated frequencies. Bi-spectrum analysis has been performed to examine the coupling between different frequencies present in the signal. Bi-spectrum (shown in the bottom panel of Figure 7) clearly shows that the Doppler frequencies (15 and 15.25 Hz) are independent and come from discrete sources. We have also examined the interaction between the signals having Doppler shifts of 15 and 15.25 Hz with respect to coupling term of the bi-spectrum. These coupling effects are expected to occur at 0.25 Hz (15.25–15 Hz) and 30.25 Hz (15.25 + 15 Hz). We found that the amplitudes of the coupling terms (not presented here) for 0.25 and 30.25 Hz are insignificant and hence the observed spectral broadening and multi-peaks are related to discrete localized targets.

Although these results cannot be compared directly with many of the present-day results based on radar imaging techniques, some of the important results obtained in the past experiments using radar of similar wavelength are worth mentioning. For example, Thompson⁴ interpreted the high returns at 7.5 m wavelength from lunar highlands as due to scattering from large blocks at significant depths within the low-loss anorthositic megaregolith. On the other hand, Campbell *et al.*⁶ found that radar observations at 7.5 m wavelength differed on several counts from those of centimetre scales. They inferred that abundance of ilmenite within the regolith and basal lava flows does not greatly affect the 7.5 m echoes. They also inferred that strong echoes are controlled by the age of the mare basalt flows, with older deposits having greater degree of

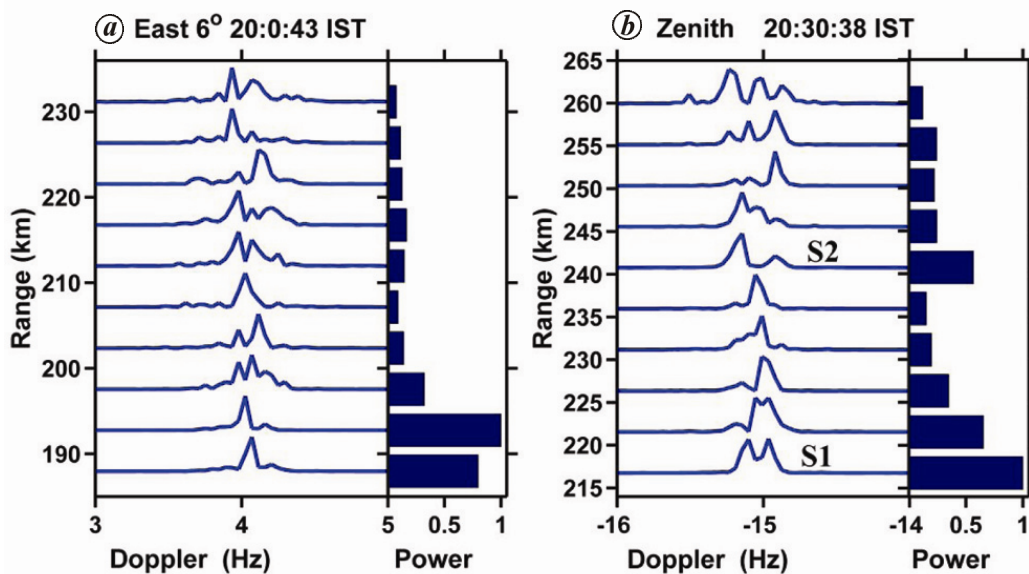


Figure 6. Variations of spectral features with range observed in (a) East-6° and (b) zenith beams. Histograms on the right show normalized echo power. S1 and S2 represent spectra for further analysis.

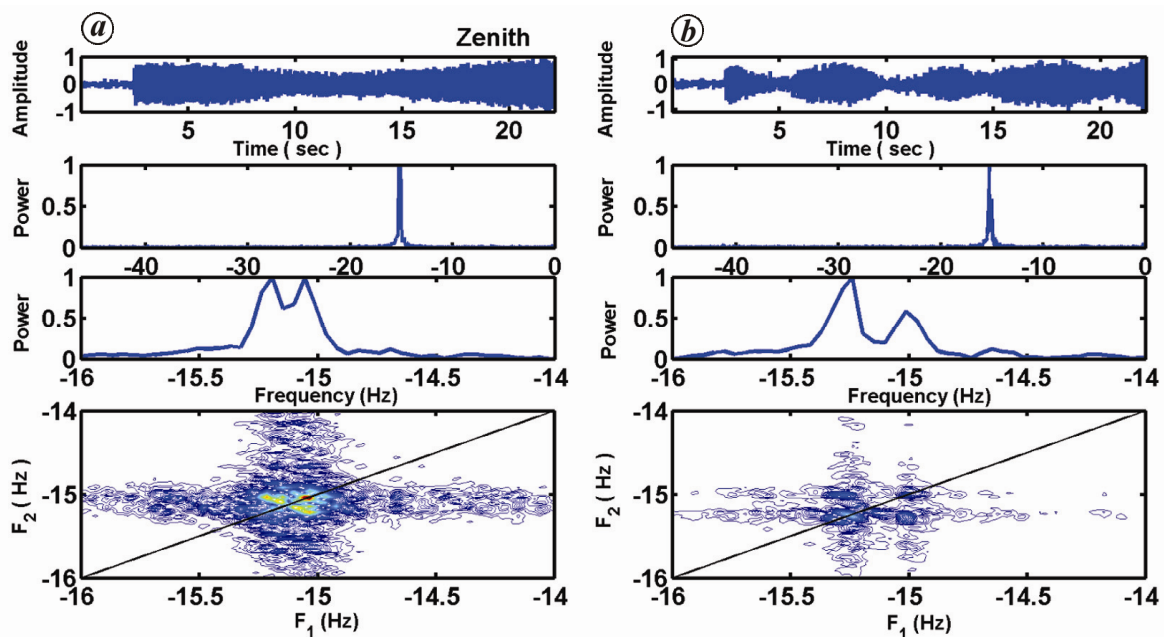


Figure 7. Time series of signal amplitude in the in-phase channel (top panel), power spectrum (second panel), zoomed version of the power spectrum (third panel), and bi-spectrum (bottom panel) corresponding to the echoes marked as (a) S1 and (b) S2 in Figure 6b.

fracturing and higher backscatter. In this context, mapping of the Moon by employing the delay-Doppler technique¹⁸ on the Gadanki MST radar would be interesting. To the best of our knowledge, high-resolution mapping of the Moon has not been done by such MST radars. Employment of the delay-Doppler technique on the Gadanki MST radar would be a reality in the near future once the existing system is upgraded to incoherent scatter radar, which will

provide circular polarization to avoid Faraday rotation and coded long pulse, a project that is currently in progress. We propose to use coded long pulse and delay-Doppler technique¹⁷ for high-resolution mapping the Moon surface. It is hoped that such observations can be compared with those of Mini-SAR on-board *Chandrayaan-1* (refs 7, 10), not only to understand the Moon surface but also to study the VHF echoes from the Moon and ionospheric effects.

Summary and concluding remarks

We have demonstrated that the 53 MHz Gadanki MST radar is capable of detecting Moon echoes. Salient results obtained are: (1) the Moon echoes are found to have SNR as high as 20 dB; (2) echo power changes as the radar pulse travels from the sub-terrestrial point towards the limbs consistent with the angular dependence of echo power; (3) Doppler spectral property changes from narrow single-peak spectrum to multi-peak spectrum as the radar pulse travels from the sub-terrestrial point towards the limbs, and (4) multi-peak spectra are found to be originating from multiple discrete targets on the Moon. The Moon echoes could be effectively used to calibrate the antenna pattern of the Gadanki MST radar. We have also outlined the potential application of the radar in high-resolution mapping of the Moon and other planetary bodies in near future.

1. DeWitt, J. H. and Stodola, E. K., Detection of radio signals reflected from the moon. *Proc. IRE*, 1949, **37**, 229–242.
2. Evan, J. V. and Pettengill, G. H., The scattering behavior of the moon at wavelengths of 3.6, 68 and 784 centimeters. *J. Geophys. Res.*, 1963, **68**(2), 423–447; doi:10.1029/JZ068i002p00423.
3. Thompson, T. W., Atlas of lunar radar map at 70-cm wavelength. *Earth Moon Planets*, 1974, **10**, 87–117; doi:10.1007/BF00562019.
4. Thompson, T. W., High resolution lunar radar map at 7.5 meter wavelength. *Icarus*, 1978, **36**, 174–188; doi:10.1016/0019-1035(78)90102-1.
5. Margot, J. I., Campbell, D. B., Jurgens, R. F. and Slade, M. A., Topography of the lunar poles from radar interferometry: a survey of cold trap locations. *Science*, 1999, **284**, 1658–1660; doi:10.1126/science.284.5420.1658.
6. Campbell, B. A., Hawke, B. R. and Thompson, T. W., Regolith composition and structure in the lunar maria: results from long-wavelength radar studies. *J. Geophys. Res.*, 1997, **102**, 19307–19320; doi:10.1029/97JE00858.
7. Spudis, P. D. *et al.*, Initial results for the north pole of the moon from Mini-SAR, Chandrayaan-1 mission. *Geophys. Res. Lett.*, 2010, **37**, L06204; doi:10.1029/2009GL042259.
8. Nozette, S. *et al.*, The Clementine bistatic radar experiment. *Science*, 1996, **274**, 1495–1498; doi: 10.1126/science.274.5292.1495.
9. Stacy, N. J. S., Campbell, D. B. and Ford, P. G., Arecibo radar mapping of the lunar poles: a search for ice deposits. *Science*, 1997, **276**, 1527–1530; doi:10.1126/science.276.5318.1527.
10. Fa, W., Wieczorek, M. A. and Heggy, E., Modeling polarimetric radar scattering from the lunar surface: study on the effect of physical properties of the regolith layer. *J. Geophys. Res.*, 2011, **116**, E03005; doi:10.1029/2010JE003649.
11. Klemperer, W. K., The angular scattering law for the moon at 6 meters wavelength. *J. Geophys. Res.*, 1965, **70**(15), 3798–3800; doi:10.1029/JZ070i015p03798.
12. Davis, J. R. and Rohlf, D. C., Lunar radio-reflection properties at decimeter wavelengths. *J. Geophys. Res.*, 1964, **69**(15), 3257–3262.
13. Fukao, S., Sato, T., Tsuda, T., Yamamoto, M., Yamanaka, M. D. and Kato, S., MU radar: new capabilities and system calibrations. *Radio Sci.*, 1990, **25**, 477–485.
14. Fukao, S. *et al.*, Equatorial Atmosphere Radar (EAR): system description and first results. *Radio Sci.*, 2003, **38**(3), 1053; doi:10.1029/2002RS002767.
15. Rao, P. B., Jain, A. R., Kishore, P., Balamuralidhar, P., Damle, S. H. and Viswanathan, G., Indian MST radar system 1, system description and sample wind measurements in ST mode. *Radio Sci.*, 1995, **30**, 1125–1138.
16. Patra, A. K., Anandan, V. K., Rao, P. B. and Jain, A. R., First observations of equatorial spread F from Indian MST radar. *Radio Sci.*, 1995, **30**, 1159–1165.
17. Davis, J. R., Rohlf, D. C., Skaggs, G. A. and Joss, J. W., Decimeter-wave radar studies of the lunar surface. *J. Res. Natl. Bur. Stand., Sec. D.*, 1965, **69**, 1659–1667.
18. Pettengill, G. H., Zisk, S. H. and Thompson, T. W., The mapping of lunar radar scattering characteristics. *Moon*, 1974, **10**, 3–16.

ACKNOWLEDGEMENT. We thank the MST radar staff for their support in conducting the Moon echo experiment.

Received 7 July 2015; revised accepted 4 April 2016

doi: 10.18520/cs/v111/i1/141-146